International Symposium
On Turbulence and Shear Flow
Phenomena (TSFP-8)
August 28 - 30, 2013 Poitiers, France

DNS OF TURBULENT CHANNEL FLOW OVER ENGINEERING ROUGH SURFACES

Angela Busse, Chris J. Tyson, and Neil D. Sandham
Faculty of Engineering and the Environment
University of Southampton
United Kingdom
a.busse@soton.ac.uk, cjt106@soton.ac.uk, n.sandham@soton.ac.uk

Mark Lützner
Institut für Aerodynamik und Gasdynamik
Universität Stuttgart
Germany

ABSTRACT

Most rough surfaces found in engineering applications are irregular and possess features on multiple length scales. In these respects they differ considerably from standard roughness models, such as arrays of cubes, used in most experiments and numerical simulations investigating turbulent flow over rough surfaces. Results from direct numerical simulations of turbulent channel flow at $Re_\tau = 180$ over realistic representations of typical engineering rough surfaces are presented in this paper. The surface geometries are based on surface scans of four different materials: graphite, carbon-carbon composite, shotblasted and ground steel. The roughness function ΔU^+ shows a strong dependence on the three-dimensional topography of the surfaces and is not solely determined by the physical roughness height. The dependence of the roughness function on various characteristic topological surface parameters has been tested. As expected, the roughness function increases with the surface skewness and the effective slope. It is also found that the roughness function decreases with increasing surface bearing index. The surface anisotropy and the texture direction of the surface with respect to the mean flow direction has an additional effect on the roughness function. Of the normal Reynolds stresses, only the streamwise stress shows a clear correlation to the degree of roughness of the surface. The spanwise and wall-normal stresses are largely unaffected by the degree of roughness and the roughness type outside the roughness sub-layer.

INTRODUCTION

Many turbulent flows occurring in engineering applications or in the natural environment are influenced by the presence of roughness on their boundaries. The roughness of a surface can be a side-effect of the production process (Langelandsvik *et al.* (2008)) or can develop over time as a result of wear and damage or contamination as, e.g. in the case of turbine blades (Bons *et al.* (2001)). In many cases surfaces are made deliberately rough in order to improve their properties in some respect. Self-cleaning surfaces contain roughness to imitate the Lotus effect, porous surfaces are used to reduce noise and riblets can be employed for drag reduction (Boorsma *et al.* (2010); Choi *et al.* (2012)). In the natural environment rough surfaces are the norm rather than the exception, and roughness can be found on many scales ranging from sand grains to urban canopies (Hewitt & Jackson (2009)).

Most previous laboratory and numerical investigations of the fundamental properties turbulent flow over rough surfaces have concentrated on surfaces constructed from simple elements, such as cubes, bars and spheres, usually arranged in a regular pattern. However, most rough surfaces encountered in practical applications are irregular and contain features of a range of different sizes. They bear only limited resemblance to the above-mentioned artificially constructed rough surfaces.

The aim of this project is to simulate turbulent channel flow over more realistic approximations of naturally occurring rough surfaces, and to identify how much the individual surface topographies affect the flow properties.

NUMERICAL METHOD

A simple three-step process has been developed which can be used to obtain the aerodynamic properties of a rough surface. First, a surface sample is scanned, e.g. using a microscope. In the current study an Alicona InFinite Focus microscope has been used. In the following surface processing step the data is filtered in order to remove measurement noise and features on very small scales. In the final step the filtered surfaces are used as solid boundary conditions in direct numerical simulations of turbulent channel flow. The aerodynamic properties of the surface can then be evaluated from the resulting mean flow and turbulence statistics.

Surface Processing

The surface data acquisition step gives a three-dimensional discrete map of surface height as a function of two coordinates, $h(x_i, y_i)$, where $x_i = 0, \Delta s, 2\Delta s, \ldots, (M-1)\Delta s$ is the streamwise and $y_i = 0, \Delta s, 2\Delta s, \ldots, (N-1)\Delta s$ is the spanwise coordinate. An example is shown in figure 1

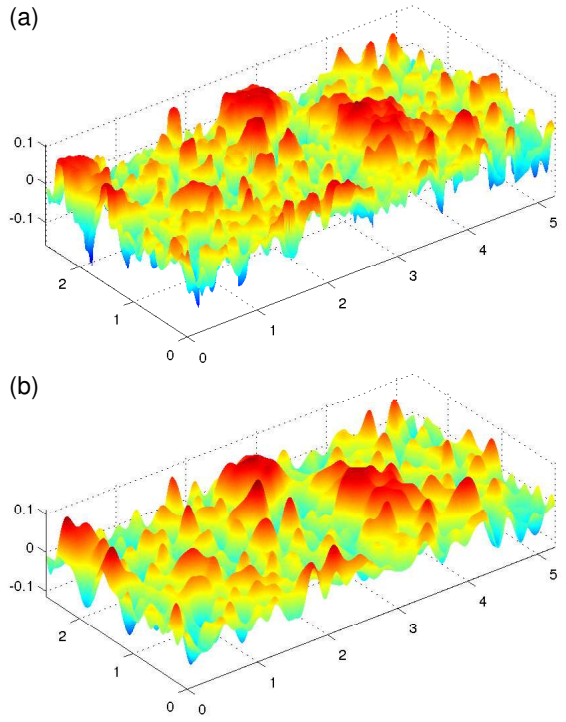

Figure 1. Example for a surface before (a) and after (b) the filtering step. The graphite surface is shown.

(a). The scanned areas have been cut to a 2 : 1 aspect ratio, i.e. the streamwise domain size L_x is twice the spanwise L_y. In all cases shown here, the spacing Δs of the sampling points is uniform and equal in the x and y directions.

The height map $h(x_i, y_i)$ cannot directly be used as a boundary condition for the direct numerical simulations since, firstly, a full resolution of all surface features would usually be computationally too expensive. Secondly, the simulations of fully developed turbulent channel flow are most efficient when periodic boundary conditions are used in the streamwise and spanwise directions of the channel. However, in general a surface scan $h(x_i, y_i)$ will not be periodic. If a channel was directly tiled with the surface map, abrupt jumps in the surface height would occur at the tile edges. Therefore, some degree of preprocessing is required.

In the current study, a circular low-pass Fourier filter is employed in order to obtain a computationally manageable and smoothly varying periodic surface $g(x, y)$. First, the discrete Fourier transform of the original height map $\tilde{h}(k_x, k_y)$ is found. Here $k_x = \frac{p}{\Delta s M}$ and $k_y = \frac{q}{\Delta s N}$ are the streamwise and spanwise components of the two-dimensional wave-vector, where $p = -\frac{M}{2}, -\frac{M}{2}+1, \ldots, \frac{M}{2}-1$ and $q = -\frac{N}{2}, -\frac{N}{2}+1, \ldots, \frac{N}{2}-1$. The discrete Fourier transform of the filtered height map is then given by

$$\tilde{g}(k_x, k_y) = \tilde{h}(k_x, k_y) f_c(k_x, k_y) \tag{1}$$

where

$$f_c(k_x, k_y) = \begin{cases} 1 & \text{for} \quad k_x^2 + k_y^2 \leq k_c^2, \\ 0 & \text{for} \quad k_x^2 + k_y^2 > k_c^2. \end{cases} \tag{2}$$

Here, $f_c(k_x, k_y)$ is the filter function and k_c is the cut-off wavenumber. The filtered surface is then represented by an exact analytic function $g(x, y)$, i.e. a sum of Fourier modes, and thus can be used to describe the boundary at any level of resolution required. An example for a filtered surface is shown in figure 1 (b). Although the filtered surface has lost some small-scale features compared to the original surface it still bears a strong resemblance to it.

The level of filtering needs to be adapted to a given surface. A too strong level of filtering can strongly distort or remove important characteristics of a surface, whereas a too low level of filtering results in a surface with an unmanageable level of detail.

Flow Simulation

The incompressible Navier-Stokes equations are solved using a standard second order finite difference scheme which operates on a staggered Cartesian grid. For time integration a second order Adams-Bashforth method is used. Periodic boundary conditions are employed in the streamwise and spanwise directions. The turbulent flow is driven by a constant mean streamwise pressure gradient. The Reynolds number based on the effective wall shear stress is $Re_\tau = 180$ in all cases shown here.

The same rough surface pattern is applied at the lower and the upper boundary of the channel. The upper surface corresponds to a mirror image of the lower surface and is shifted by $L_x/2$ in the streamwise and $L_y/2$ in the spanwise direction relative to the lower surface. The mean channel height is set to $L_z = 2$. The irregular rough walls of the channel are resolved using an immersed boundary method, which employs an extra forcing term at grid points adjacent to the boundary to enforce zero velocity at the walls. Within the walls, the flow velocity is set to zero. The immersed boundary method used here is an iterative formulation of the method of Yang & Balaras (2006); it has been validated using a number of rough-wall related test cases, such as turbulent channel flow over a wavy wall (Maaß & Schumann (1996)).

The Cartesian grid is stretched in the wall-normal direction in order to give a higher resolution in the region of the rough walls and a larger spacing towards the channel centre. Across the full height of the roughness a uniform spacing $\Delta z^+_{\text{min}} < 1$ is used. A uniform grid spacing is also used in the streamwise and spanwise direction. Details of domain sizes and grid spacings are given in table 1.

Table 1. Simulation parameters

surface type	$L_x \times L_y$	Δx^+	Δy^+	Δz^+_{min}
smooth	10×4	11.25	5.625	0.75
graphite	5.25×2.625	2.46	2.46	0.67
composite	9.8×4.9	4.59	4.59	0.67
ground	23.2×11.6	5.44	5.44	0.67
shotblasted	17.5×8.75	4.92	4.92	0.67

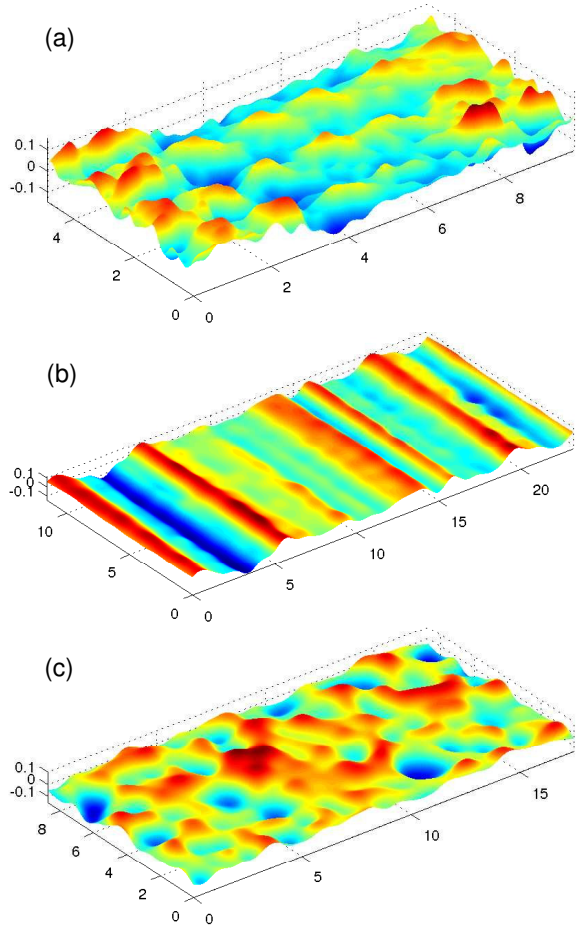

Figure 2. Surfaces used in the study: (a) composite material, (b) ground steel, (c) shotblasted steel. All surfaces have been filtered. The graphite sample is shown in figure 1(b).

SURFACE SAMPLES

Four different surface samples have been used in the present study. The graphite and (carbon-carbon) composite surfaces have been exposed to arc-heating, while the shotblasted and ground steel surfaces have been taken from standard roughness comparators.

All surfaces have been scaled to give the same mean peak to valley height[1] $S^+_{z,5\times5} \approx 30$, to have a comparable roughness height in all cases. $S_{z.5\times5}$ has been chosen as the reference roughness height, since the largest roughness features of a surface are known to have the strongest effect on the flow (Colebrook & White (1937); Jiménez (2004)). It is therefore in the fluid dynamic context a more suitable measure of the roughness height than the mean roughness amplitude S_a or the root-mean square deviation of the surface S_q.

Due to the different surface topographies different domain sizes have been used for different samples. A rather small domain size resulted for the graphite sample. However, the turbulent flow over this surface is strongly influenced by the roughness and the velocity correlations decay rapidly in the streamwise and spanwise directions, indicating that the domain size is still sufficiently large.

[1]For the computation of $S_{z,5\times5}$ a surface is partitioned into 5 by 5 sections. For each section the maximum and minimum surface height is found. The mean peak to valley height is then defined as the difference between mean of the maxima and the mean of the minima.

Table 2. Characteristic surface parameters: mean peak-to-valley height $S_{z,5\times5}$, average surface amplitude S_a, root mean square deviation of surface S_q, surface skewness S_{sk}, surface flatness S_{ku}, shortest correlation length S_{al}, surface texture aspect ratio S_{tr}, surface bearing index S_{bi}.

parameter	graph	comp	ground	shotbl
$S_{z,5\times5}$	0.167	0.167	0.166	0.166
S_a	0.029	0.035	0.041	0.032
S_q	0.037	0.044	0.051	0.041
S_{sk}	0.28	0.24	−0.13	−0.41
S_{ku}	2.97	2.87	2.82	3.38
S_{al}	0.22	0.57	0.95	0.94
S_{tr}	0.61	0.29	0.08	0.93
S_{bi}	0.53	0.57	0.62	0.65

The different surfaces used in the following are illustrated in figures 1 (b) and 2 (a) to (c). Key surface parameters are given in Table 2. Their definitions can be found in Mainsah *et al.* (2001). From the illustrations and surface texture aspect ratio S_{tr} it can be inferred that the graphite and the shotblasted steel surface can be regarded as approximately isotropic surfaces ($S_{tr} > 0.5$) whereas the composite and the ground steel surfaces are anisotropic. The ground steel shows the highest degree of anisotropy with clearly developed spanwise grooves. The anisotropy of the composite sample is less pronounced; for this sample the features tend to be aligned in the streamwise direction. The height distributions show distinctive variations in skewness factors. In the case of the graphite and composite samples a positive skewness is found, indicating the presence of narrow peaks. For the shotblasted steel surface a negative skewness is found which corresponds to the flatter peaks which can be observed in this case. In comparison, the flatness factors of the height distributions do not show large differences and are close to Gaussian in all cases.

RESULTS

The mean streamwise velocity profiles for the different rough surfaces and the smooth wall reference case are shown in figure 3. All the rough surfaces have a clear effect on the mean flow. Outside the roughness layer the mean streamwise velocity is reduced compared to the reference case. The strength of the roughness effect can be measured using ΔU^+, i.e. the downwards shift in the velocity profile. Due to the low Reynolds number of this study no clearly established log region can be observed in the velocity profile. Therefore ΔU^+ is estimated by subtracting the respective centreline velocity from the centreline velocity of the reference case (Busse & Sandham (2012)). The values for ΔU^+, listed in table 3, all fall into the transitionally rough region and vary from 1.42 to 4.78. Although all rough surfaces have been scaled to the same roughness height $S_{z,5\times5}$, the spread in the ΔU^+ values is significant. The graphite surface gives a ΔU^+ of 4.78 which is more than three times

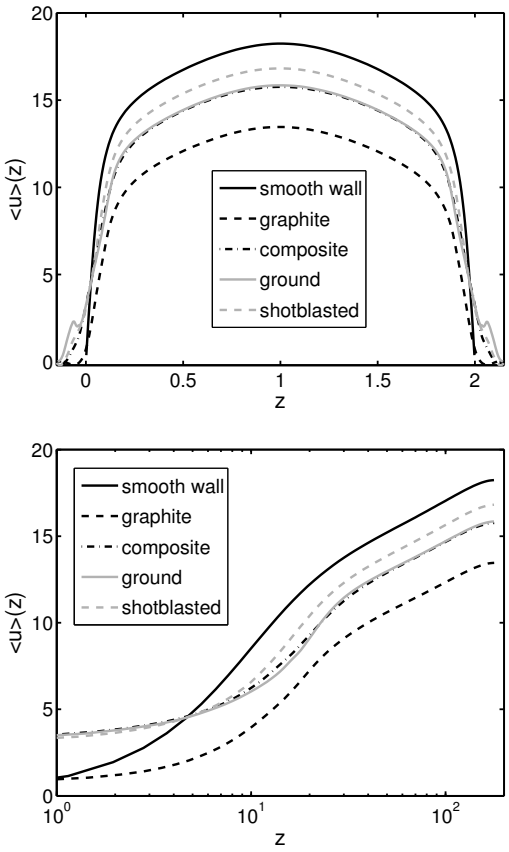

Figure 3. Mean streamwise velocity versus distance from the wall. In the rough wall cases the mean roughness plane is used as the wall location.

Table 3. Measured value of the roughness function ΔU^+.

parameter	graph	comp	ground	shotbl
ΔU^+	4.78	2.48	2.39	1.42

the ΔU^+ value caused by the shotblasted surface. In contrast, the composite and the ground steel surface give very similar ΔU^+ values which fall in between these extremes.

A number of models that correlate the three-dimensional topological characteristics of a surface to ΔU^+ or the equivalent sand grain roughness k_s have been proposed (Flack & Schultz (2010)). In most cases, they are applicable to the fully rough regime. In absence of models for the transitionally rough regime some of these correlations will be tested in the following. Flack & Schultz proposed an empirical formula that states that k_s (and therefore ΔU^+) should increase with both the root-mean-square roughness height S_q and the surface skewness S_{sk}. As can be inferred from tables 2 and 3, for the present cases ΔU^+ does not rise with S_q. This can be explained by the fact that the rough surfaces have already been scaled to give the same $S_{z,5\times5}$ and thus the difference in S_q between the surfaces is already small. An increase of ΔU^+ with increasing surface skewness can be observed (see figure 4 (a)). However, there is a significant difference in the skewness values of the composite and the ground steel surface, but only a very small difference in their roughness function ΔU^+. The high anisotropy of the ground steel surface combined with the alignment of its texture direction with the spanwise direction appears to induce an additional roughness effect which cannot be captured by S_{sk}.

Napoli *et al.* (2008) proposed the effective (streamwise) slope as a measure for the aerodynamic roughness of two-dimensional rough surfaces, i.e. surfaces with no spanwise variation. This parameter can be extended to general three-dimensional rough surfaces by

$$ES_x = \frac{1}{A_S}\int_S \frac{\partial g(x,y)}{\partial x} dA \qquad (3)$$

where $g(x,y)$ is the function describing the surface S and A_S is the projected surface area. ΔU^+ increases with increasing effective streamwise slope ES_x (see figure 4 (b)). Despite a significant difference in ΔU^+, the ES_x-value of the ground steel surface is not much higher than the corresponding value for the shotblasted surface. This can again be attributed to the fact that the ES_x-parameter does not contain any information about the spanwise surface topography and thus cannot capture surface anisotropy effects. Another parameter that shows a variation with ΔU^+ is the surface bearing index S_{bi} (see figure 4 (c)). The surface bearing index is the ratio of the rms surface deviation over the surface height at which 5% of the surface area is revealed. ΔU^+ decreases with increasing surface bearing index S_{bi}. The surface bearing index S_{bi} could be used as a measure for the solidity of a rough surface. In the limit of high solidities, the roughness of a surface is known to decrease with solidity (Jiménez (2004)).

Rough surfaces are also known to have a strong effect on the turbulence properties of the flow. The peak of the streamwise Reynolds stress, shown in figure 5, is reduced by the presence of the roughness. As expected (see e.g. Krogstad *et al.* (2005)) the damping of the peak is stronger with increasing roughness function. In the middle of the channel the streamwise Reynolds stress profile approximately collapses onto the smooth-wall reference case.

An increased peak value of the spanwise and a decreased peak value of the wall-normal Reynolds stress can be observed. In the central area of the channel the level of wall-normal and spanwise velocity fluctuations is elevated compared to the smooth wall reference case. Outside the layer directly affected by the rough surface, the profiles for all rough surfaces collapse, i.e. no dependence on ΔU^+ or the individual roughness type can be observed.

In the context of cube and bar-shaped roughness a correlation between ΔU^+ and the level of the wall-normal velocity fluctuations has been found by Orlandi & Leonardi (2008): the roughness function increases linearly with the mean wall-normal Reynolds stress in the crest plane of the roughness. Since for the irregular roughness studied here no unique crest plane exists, we use the surface bearing height $\eta_{0.05} = S_q/S_{bi}$ as the reference plane. ΔU^+ versus the level of wall-normal velocity fluctuations in the reference plane is shown in figure 6. For the present cases the correlation of Orlandi & Leonardi (2008) does not hold. This is probably due to the strong difference between the irregular rough surfaces studied here and rough surfaces which have been constructed using cube and bar-shaped roughness elements.

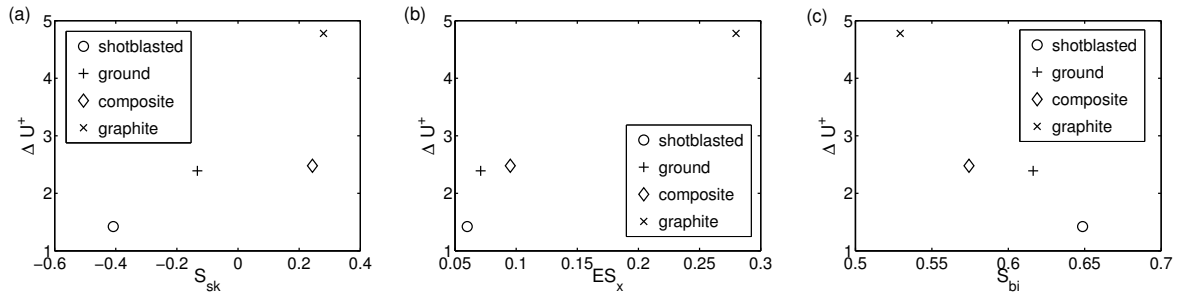

Figure 4. Roughness function ΔU^+ versus topological surface parameters: (a) surface skewness, (b) effective streamwise slope, (c) surface bearing index.

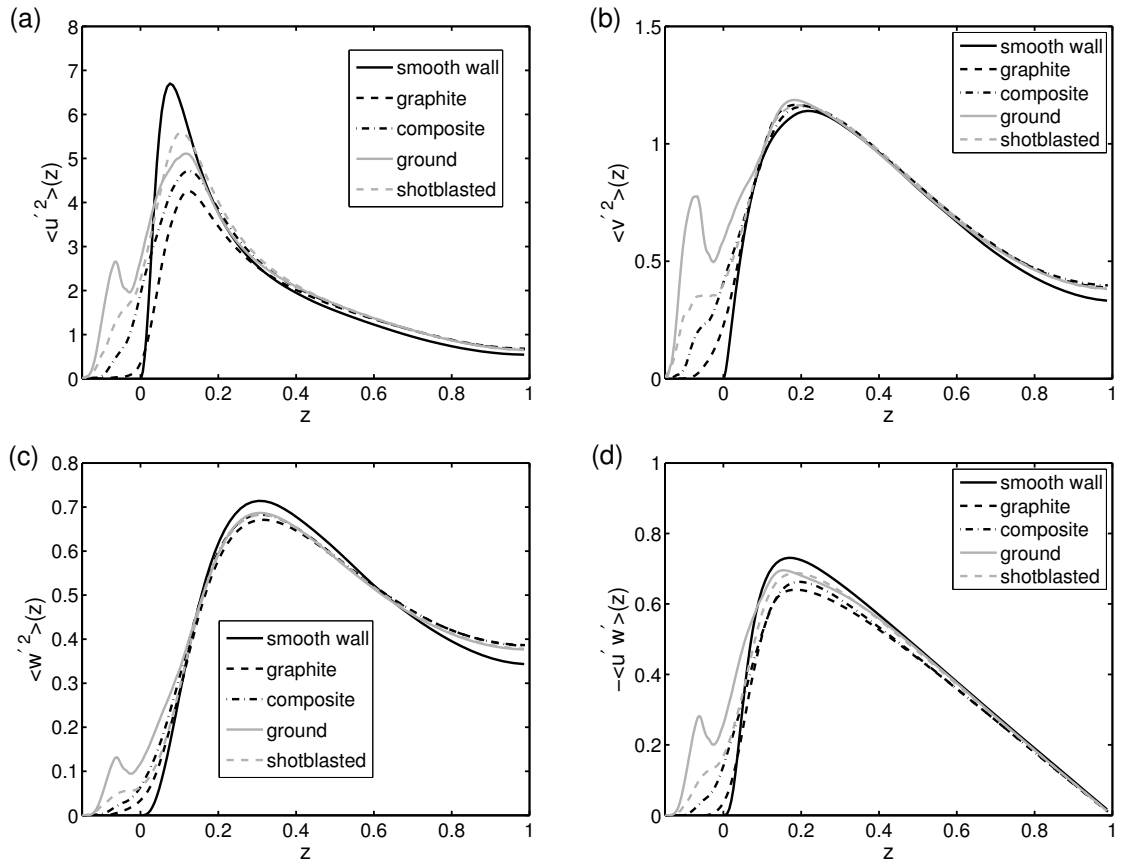

Figure 5. (a) Streamwise, (b) spanwise, (c) wall-normal Reynolds stress and (d) Reynolds shear stress.

SUMMARY AND OUTLOOK

A method has been presented by which the aerodynamic properties of a rough surface can be determined using direct numerical simulations. Results were shown for four different engineering rough surfaces. For same physical roughness height a strong spread in the aerodynamic roughness of the surfaces was found, indicating that the individual three-dimensional surface topographies have a strong influence on the effective friction factor. The correlation of the resulting roughness function values ΔU^+ to various characteristic surface parameters has been tested. In agreement with the observations of Flack & Schultz (2010) and Napoli *et al.* (2008) an increase of ΔU^+ with decreasing surface skewness and increasing effective slope was found. Furthermore it was observed that ΔU^+ decreased with increasing surface bearing index. A comparison of the composite and the ground steel surface showed that the surface anisotropy and the texture direction of the surface with respect to the mean flow direction have additional influence on the roughness function. These effects cannot be captured by parameters such as the surface skewness, effective slope and surface bearing index which are based on the surface height probability density function.

An extension of the study to higher Reynolds numbers and into the fully rough regime is planned. Since the current study has only a small set of samples, no reliable correlations to topological surface parameters could be established. Therefore, a diverse and much larger range of samples needs to be studied to obtain reliable correlations between the topological surface parameters and the aerodynamic surface roughness.

Work is currently under the way to study the effects of irregular roughness on turbulent channel flow in the compressible case. This is of high interest in the context of reentry vehicles where roughness has a strong influence on the heat transfer (see e.g. Bianchi *et al.* (2010)). Some first

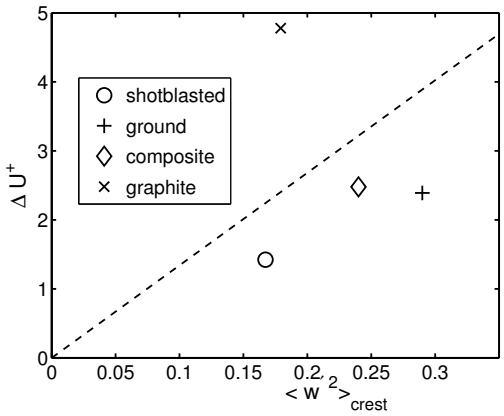

Figure 6. Roughness function ΔU^+ versus mean wall-normal Reynolds stress at the surface bearing height $\eta_{0.05}$; the dashed line shows the empirical formula of Orlandi & Leonardi (2008) which has been found in the context of cube and bar roughness.

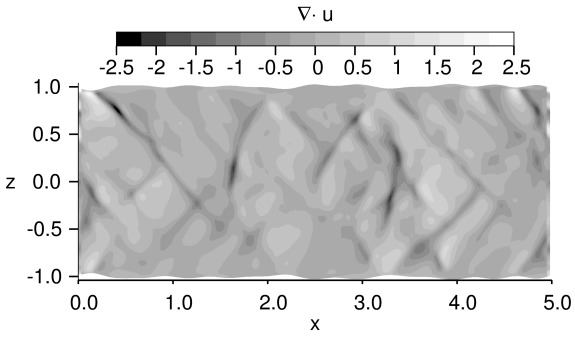

Figure 7. Instantaneous $\nabla \cdot u$ contours showing weak shock waves over a graphite based irregular roughness at a Mach number of 1.5.

results are shown in figure 7, where shock waves can be observed in turbulent channel flow over an irregular rough surface, which is based on the graphite sample. The details of the numerical method employed for this simulation can be found in Tyson & Sandham (2013).

ACKNOWLEDGEMENTS

We would like to thank Marc Zanchetta (GasDynamics, UK) and the National Physics Laboratory for providing surface data for the graphite and the composite sample. We would like to thank Dr. Jurgita Zekonyte and Liam Goodes (nCATS, UK) for their support in scanning the other samples.

REFERENCES

Bianchi, D., Nasuti, F. & Martelli, E. 2010 Navier-stokes simulations of hypersonic flows with coupled graphite ablation. *Journal of Spacecraft and Rockets* **47**, 554–562.

Bons, J. P., Taylor, R. P., McClain, Stephen T. & Rivir, R. B. 2001 The many faces of turbine surface roughness. *Journal of Turbomachinery* **123**, 739–748.

Boorsma, K., Zhang, X. & Molin, N. 2010 Landing gear noise control using perforated fairings. *Acta Mechanica Sinica* **26**, 159–174.

Busse, A. & Sandham, N.D. 2012 Parametric forcing approach to rough-wall turbulent channel flow. *J. Fluid Mech.* **712**, 169–202.

Choi, H., Park, H., Sagong, W. & Lee, S. 2012 Biomimetic flow control based on morphological features of living creatures. *Physics of Fluids* **24**, 121302.

Colebrook, C. F. & White, C. M. 1937 Experiments with fluid friction in roughened pipes. *Proc. Roy. Soc. Lond. A* **161**, 367–381.

Flack, K. A. & Schultz, M. P. 2010 Review of hydraulic roughness scales in the fully rough regime. *Journal of Fluids Engineering* **132**, 041203.

Hewitt, C. N. & Jackson, A. V. 2009 *Atmospheric Science for Environmental Scientists*. Wiley.

Jiménez, J. 2004 Turbulent flow over rough walls. *Annu. Rev. Fluid Mech.* **36**, 173–96.

Krogstad, P.-A., Andersson, H. I., Bakken, O. M. & Ashrafian, A. 2005 An experimental and numerical study of channel flow with rough walls. *J. Fluid Mech.* **530**, 327–352.

Langelandsvik, L. I., Kunkel, G. J. & Smits, A. J. 2008 Flow in a commercial steel pipe. *J. Fluid Mech.* **595**, 323–339.

Maaß , C. & Schumann, U. 1996 *Notes on numerical fluid mechanics, vol. 52*, pp. 227–41. Vieweg.

Mainsah, E., Greenwood, J. A. & Chetwynd, D. G., ed. 2001 *Metrology and Properties of Engineering Surfaces*. Kluwer Academic Publishers.

Napoli, E., Armenio, V. & De Marchis, M. 2008 The effect of the slope of irregularly distributed roughness elements on turbulent wallbounded flows. *Journal of Fluid Mechanics* **613**, 385–394.

Orlandi, P. & Leonardi, S. 2008 Direct numerical simulation of three-dimensional turbulent rough channels: parameterization and flow physics. *J. Fluid Mech.* **606**, 399–415.

Tyson, C. J. & Sandham, N. D. 2013 Numerical simulation of fully-developed compressible flows over wavy surfaces. *Int. J. Heat Fluid Flow* (in press).

Yang, J. & Balaras, E. 2006 An embedded-boundary formulation for large-eddy simulation of turbulent flows interacting with moving boundaries. *J. Comput. Phys.* **215**, 12–40.